



Mineralogy, geochemistry and origin of the phosphorites at Um El-Huwat mine, Quseir, Central Eastern Desert, Egypt

Esmat A. Abou El-Anwar¹ · Said H. Abd El Rahim¹

Accepted: 10 January 2022 / Published online: 11 February 2022
© The Author(s) 2022

Abstract

X-Ray diffraction results for the study mine are mainly represented by two phases (phosphatic and non-phosphatic). First phase is represented by apatite (fluorapatite) which is the dominant. The second phase includes carbonate minerals; calcite, dolomite, evaporated mineral (gypsum), sulphide mineral (pyrite), in addition to quartz as a silicate mineral. These results are confirmed by the petrographic study. The detailed microscopic examinations indicate that the phosphorites at the study mine is essentially composed of phosphatic lithoclasts (mainly collophane), phosphatic bioclasts (bone fragments, spines and teeth of vertebrates such as shark fish as well as coprolites), opaques, and quartz embedded in a microcrystalline phosphatic matrix (contains some of dahllite) associated with a microcrystalline quartz according to their decreasing order of abundance. The paragenetic sequence of the studied phosphorites is as follows: fluorapatite, collophane then followed by dahllite. The redox-sensitive trace elements, its ratios, authigenic uranium as well as Fe/Ti can be signifying the redox conditions. Also, they revealed that the study rocks are deposited under the oxic to anoxic environment coupled with hydrothermal solution. The trace and rare earth elements are generally associated with phosphatic rocks. Thus, the phosphatic rocks of Um El-Huwat mine, Quseir can be considered as sources of trace and rare earth elements. Also, pyrite can be considered as another possible source for REEs. The studied phosphatic rocks characterized by light REE (LREE = 69 ppm) enrichment than heavy REE (HREE = 25 ppm). All the recoded values of the heavy metals for the study mine are higher than those in Tunisia (400.3 ppm), Morocco (571.75 ppm) and Jordan (187 ppm). The post-depositional conditions are responsible for the enrichment of U and Th and/or intensive chemical weathering in Quseir area. Enrichment Factor (EF) indicated that the enrichment or deletion of the elements may be a function of that association and the origins of the various phosphate fractions. The studied phosphatic rocks are suitable for industrialized fertilizers according to the world guides.

Keywords Fluorapatite · Anoxic · Oxic · REE · Redox elements

Introduction

The most important factors control the mineral composition of the phosphate rocks is type and source. They are classified into four groups. They are sedimentary marine origin (75%), igneous origin (15–20%), metamorphic and weathered origin (8%), and 2–3% as biogenic sources (Ozer et al. 2000). Silica, clayey and calcareous materials are gangue minerals for the sedimentary phosphate origin. The most sedimentary calcareous phosphate rocks have been significant quantities of carbonates and are considered as carbonate-apatite or

francolites. Phosphorites are sedimentary rocks that contain more than 18–20% P_2O_5 . Most phosphorites are of marine origin. Francolite (carbonate–fluorapatite) is the main phosphate mineral. (Sengul et al. 2006).

The phosphatic rocks are mainly consisted of authigenic peloids and bioclasts. Peloids are considered as authigenic or reworked in origin (El-Kammar et al. 1979; Glenn and Arthur 1990). The formation of phosphorites may be carried nutrients from deep water into the photic zone (El-Tarabili 1969), formed in situ (Youssef 1957) or fluvial input (Glenn and Arthur 1990). The phosphorite beds of the Duwi Formation intercalated with the siliciclastic facies represented the early transgressive stage, which is characterized by the dominance of detrital input (Said 1990). The Egyptian phosphates are shallow marine sediments, whereas the maximum thickness was associated with a transgressive shoreline

✉ Said H. Abd El Rahim
said_abdelrahim@yahoo.com

¹ Geological Sciences Department, National Research Centre, Dokki, Giza, Egypt

of the Sea from north to south (Late Campanian or Early Maastrichtian) (Temraz 2005). Baumiy and Toda (2005) mentioned that the phosphates of the Duwi Formation were formed from reworked older sedimentary phosphorites and biogenic sources subjected to chemical weathering. Abou El-Anwar et al. (2016) concluded the diagenetic processes of the Duwi phosphate rocks were subjected to several processes; re-crystallization, micritization, compaction, dissolution and pyritization. They were deposited under shallow reducing condition and subjected to the effects of the chemical weathering. The Duwi phosphates rocks under investigation are authigenic in origin, which is comparable to those of the Al-Hisa Phosphorite Formation in Jordan.

Abou El-Anwar et al. (2017) explain studied the paleo-weathering and provenance of the sources of the phosphate rocks of the Duwi Formation of Geble Duwi Mine in Quseir–Safaga area, and mentioned the importance in the assessment of possible radiological hazards to human health; due to the presence of uranium in the apatite structure. Abou El-Anwar (2019) indicated the importance of the Lower phosphatic member (Campanian, Upper Cretaceous), Duwi Formation resulting in relatively high enrichment of heavy metals and U content in south Esna, at the western side of the Nile Valley. In addition, she mentioned that U contents were associated with the heavy metals and trace elements during the chemical weathering under oxic conditions. Also, she concluded that the phosphatic rocks were in south Esna deposited under anoxic reducing marine environments coupled with hydrothermal solutions.

Abou El-Anwar et al. (2019b) studied the statistical result of the interrelation between P_2O_5 , F and U concentrations on Egyptian phosphate rocks and concluded that U could be fixed with the phosphatic ion, forming secondary uranium phosphate minerals such as phosphuranylite and belovite in Quseir region. In addition to uranium minerals in Safaga region contain also Uranyl carbonates and Uranyl sulfates, which had been led to the post-depositional U enrichment. The chemical data and index show that the phosphatic rocks in Safaga region are more enriched in the majority trace and rare earth elements, and are subjected to high chemical weathering than those in Quseir region.

Also, the diagenetic process used as a tool to diagnose the paleo-environmental conditions, bathymetry and oxygenation during Late Paleocene–Early Eocene in Gafsa basin.

Abou El-Anwar et al. (2020) studied the geochemical analysis of trace, rare earth elements and the petrographical for Hamadat phosphatic rocks, and indicated that the phosphatic rocks are deposited under oxic to anoxic condition. Dolomitization process plays an important role in the concentration of trace and rare earth elements in the phosphatic rocks at Hamadat Mine. Dahllite layer has a relatively higher content in most of rare earth and some of the trace elements than those in the phosphate layer, which reveal that dahllite

structure may be having the ability to scavenging them than the phosphatic construction. Also, they used the chemical index of alteration (CIA), trace elements and La/Ce ratios pointed out that these phosphatic rocks were of hydrogenous origin deposited in cold and dry climate during low weathering. In addition to they motioned that; the hydroxial-apatite can be prepared to be used as a natural row material in the biological industry according to the chemical composition.

The present study focuses on the mineralogy, petrography and geochemistry of the phosphorites at Um El-Huwat mines of the Duwi Formation at Quseir–Safaga region, in an effort to recognize their depositional environment and economic evolution.

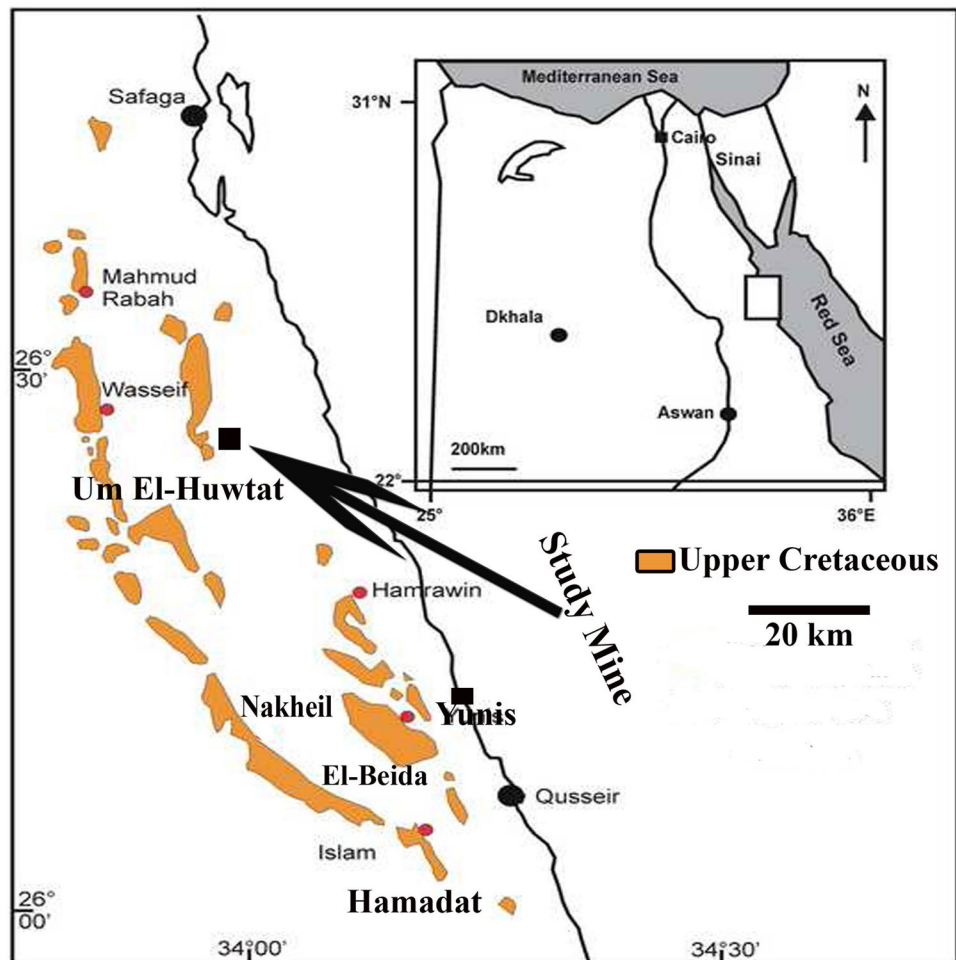
Geological setting

The sedimentary phosphatic rocks (Upper Cretaceous—Eocene) are originated in marine environments. The Mediterranean phosphatic rocks such as Egypt, Algeria, Tunisia, Jordan, Syria, Saudi Arabia, Spain, etc. are deposited in the ancient Tethyan Sea (Sengul et al. 2006). In Egypt, the phosphatic rocks for Duwi Formation are located in the Nile Valley, the Red Sea Coast, Abu Tartur plateau and Sinai. The Duwi Formation in the Quseir–Safaga region is conformably overlain by the Quseir variegated shales and underlain by the Dakhla shales (Said 1962). Duwi Formation in Egypt represents the early stage of the Late Cretaceous marine transgression. It was classified into four members according to its lithology (Baoumy and Tada 2005). The most of the phosphate beds appear as massive rocks. Their thickness up to tens of centimeters.

The chosen area is represented by Um El-Huwat mines (Fig. 1). They are occurring at the upper member of Duwi Formation in Quseir–Safaga region (Fig. 2).

Um El-Huwat mines, about 7 km from a residential village named the Um El-Huwat. This village has a big mosque and an enormous number of houses. Um El-Huwat mines have several openings, some of them are close together and the other is separated. The mines have traces of a railway line and tunnels extended to several kilometers. Phosphatic rocks in these mines extend horizontally to tens of kilometers, and range in thickness from tens of centimeters to extra meters. This layer of phosphate is confined between two-layers of the black shales. The lower layer extends along to the phosphatic bed. This layer of the black shales is homogeneous and ranges in color from light gray to dark black. Whereas the black shales overlies are ranges in color from green to red color due to the presence of the iron oxides. This succession is capped with limestone. The chosen area in Um El-Huwat mines are located at Longitudes $34^{\circ} 11' 23''$ – $34^{\circ} 11' 33''$ E and Latitudes $26^{\circ} 3' 1''$ – $26^{\circ} 3' 13''$ N (Figs. 1 and 2).

Fig. 1 The location map of the studied mine



Sampling and methodology

Geological field trips were done for studying the geologic setting and collecting fifteen representative samples of the phosphatic rocks from the area under study. Mineralogically, selected two samples were investigated by the X-ray technique at the Egyptian Mineral Resources Authority (Dokki, Egypt) using a PAN analytical X-Ray Diffraction equipment model X'Pert PRO with Secondary Monochromator, Cu-radiation ($\lambda = 1.542 \text{ \AA}$) at 45 K.V., 35 M.A. and scanning speed $0.02^\circ/\text{s}$. were used. The diffraction charts and relative intensities are obtained and compared with ICDD files. The morphology and the size of the phosphorites samples were characterized via SEM coupled with energy-dispersive spectroscopy EDX, (SEM Model Quanta FEG 250) of the two samples are carried out in the National Research Centre laboratories. Thin sections and polished surfaces were prepared for each sample. The thin sections and polished surfaces of the phosphorites were studied in detail using Transmitted Light and Reflected Light Nikon Research Polarizing Ore Microscope (Model Optiphot 2-PoL, attached with Nikon Digital Camera, Model DS-Fi2, made in Japan). Seven

samples were selected to determine the chemical composition using Axios Sequential WD-XRF Spectrometer, Analytical 2005 in the National Research Centre laboratories. ASTM E 1621 standard guide for elemental analysis by wavelength dispersive X-Ray Fluorescence Spectrometer, and ASTM D 7348 standard test methods for loss of ignition (LOI) of solid combustion.

Results and discussion

Petrographical investigation

Phosphorites are sedimentary rocks that contain more than 18–20% P_2O_5 (Sengul et al. 2006). Most phosphorites are of marine origin (Ozer et al. 2000; Bauymi and Toda 2005; Abou El-Anwar et al. 2020). Francolite (carbonate–fluorapatite) is the main phosphate mineral. Fluorapatite is most probably constituted in the biophases (bone fragments, spines and teeth of vertebrates such as shark fish as well as coprolites), (Abou El-Anwar and Sadek 2008). The detailed microscopic examinations indicate that the phosphorites at

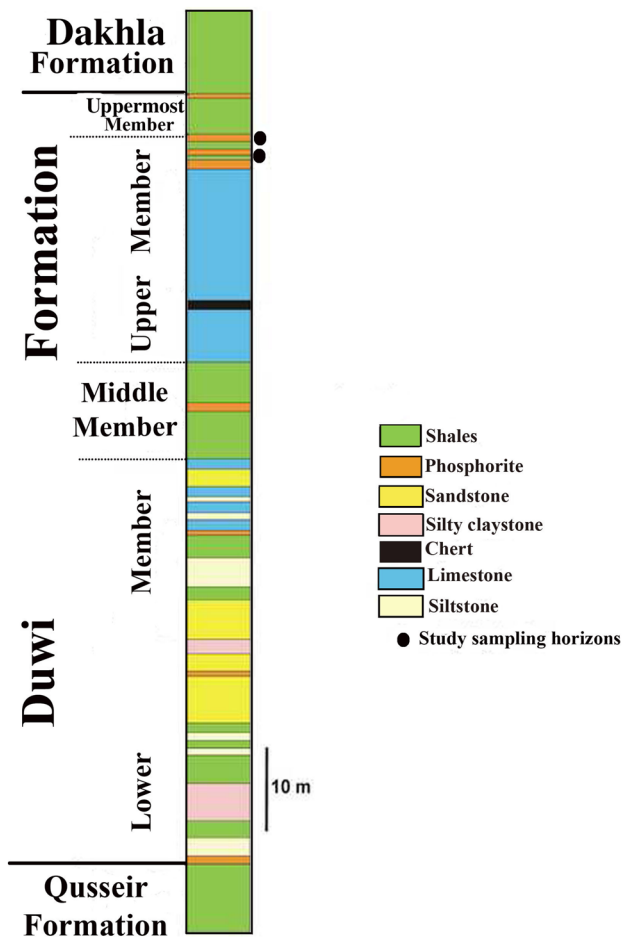


Fig. 2 Stratigraphic columnar section of the Duwi Formation in the Red Sea region (modified after Baioumy and Tada 2005)

Um El-Huwat mine, Quseir, Central Eastern Desert, Egypt is essentially composed of phosphatic lithoclasts (mainly collophane), phosphatic bioclasts (bone fragments, spines and teeth of vertebrates such as shark fish as well as coprolites), opaques, and quartz embedded in a microcrystalline phosphatic matrix (contains some of dahllite) associated with a microcrystalline quartz according to their decreasing order of abundance (Figs. 3, 4, 5, 6, 7, 8, 9 and 10). Some of calcite, dolomite and gypsum grains are commonly associated with the phosphatic phase as confirmed by X-Ray Diffraction (XRD). The paragenetic sequence of the studied phosphorites is as follows: Fluorapatite ($\text{Ca}_5(\text{PO}_4)_3\text{F}$), collophane (is an amorphous calcium carbonate-phosphate) then followed by dahllite ($3\text{Ca}_3(\text{PO}_4)_2\text{CaCO}_3$).

Fluorapatite ($\text{Ca}_5(\text{PO}_4)_3\text{F}$) occurs as colourless subhedral prismatic crystals with rectangular to acicular form (Figs. 3 and 5). It exhibits high relief. It shows parallel extinction, basal section appears dark (isotropic) between Crossed Nichols (Hexagonal Crystal System). It shows first order gray interference colours (Figs. 4 and 6).

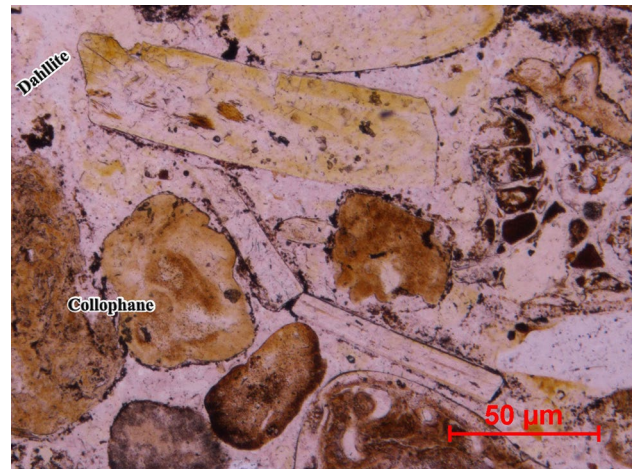


Fig. 3 Photomicrograph showing fluorapatite (colourless subhedral rectangular crystals), collophane (brown grains, pellets, spheroids, ovoids) and coprolite (brown cylindrical form) embedded in a microcrystalline matrix (colourless dahllite and quartz). Collophane is corroded and replaced by dahllite. Dahllite is growing at the expense of collophane. Phosphorite, PPL. X40

Coprolite represents fossil animal excretions that are commonly rich in organic inclusions. It occurs as cylindrical and elongated (rod like) form (Figs. 3 and 4).

Collophane is an amorphous or mineraloid calcium carbonate-phosphate. It forms brown subhedral to anhedral medium grains and aggregates; brown pellets, spheroids, ovoids are also commonly observed (Figs. 3, 5, 7 and 9). Collophane appears isotropic between Crossed

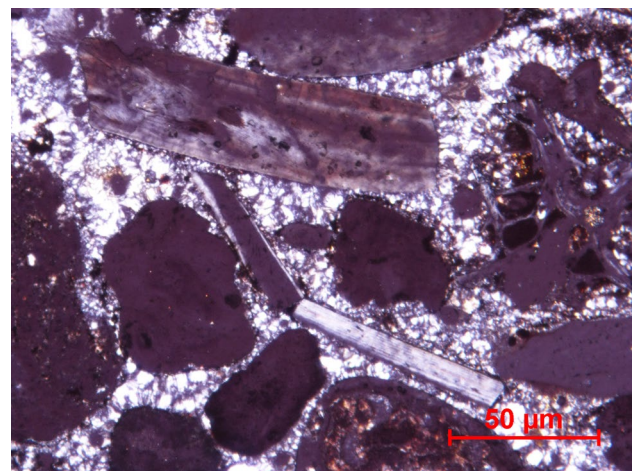


Fig. 4 Photomicrograph showing fluorapatite (subhedral rectangular crystals exhibit gray or white interference colours), collophane (isotropic grains, pellets, spheroids, ovoids) and coprolite (isotropic cylindrical form) embedded in a microcrystalline matrix (dahllite and quartz exhibit gray or white interference colours). Collophane is corroded and replaced by dahllite. Dahllite is growing at the expense of collophane. Phosphorite, C.N. X40



Fig. 5 Assemblage of fluorapatite (colourless subhedral rectangular crystals), collophane (brown grains, pellets, spheroids, ovoids), spines of vertebrates (brown) and quartz (colourless) embedded in a microcrystalline matrix (colourless dahllite and quartz). Collophane is corroded and replaced by dahllite. Dahllite is growing at the expense of collophane. Note, the spines of vertebrates were replaced by collophane. Phosphorite, PPL. X40

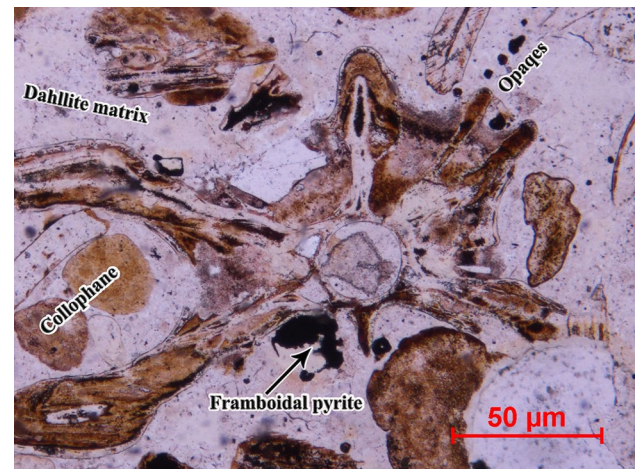


Fig. 7 Photomicrograph showing collophane (brown grains, pellets, spheroids, ovoids), opaques (dark) and quartz (colourless) embedded in a microcrystalline matrix (colourless dahllite and quartz). Framboidal pyrite scattered in the collophane. Collophane is corroded and replaced by dahllite. Dahllite is growing at the expense of collophane. Note, cross section from bony vertebrae of fish skeleton was replaced by collophane. Phosphorite, PPL. X40

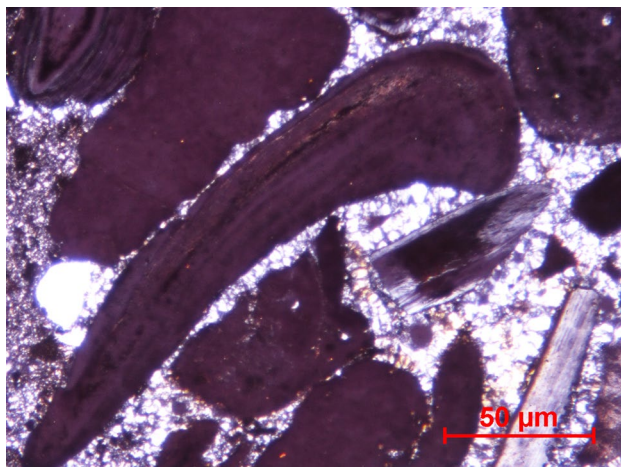


Fig. 6 Assemblage of fluorapatite (subhedral rectangular crystals exhibit gray or white interference colours), collophane (isotropic grains, pellets, spheroids, ovoids), spine of vertebrates (isotropic) and quartz (gray or white interference colours) embedded in a microcrystalline matrix (dahllite and quartz exhibit gray or white interference colours). Collophane is corroded and replaced by dahllite. Dahllite is growing at the expense of collophane. Note, the spines of vertebrates were replaced by collophane. Phosphorite, C.N. X40

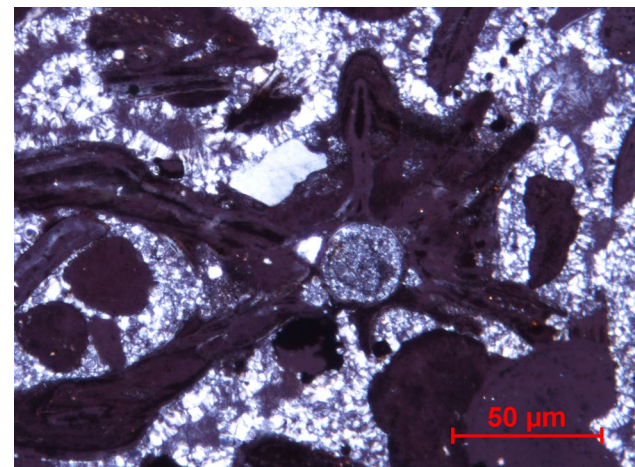


Fig. 8 Photomicrograph showing collophane (isotropic grains, pellets, spheroids, ovoids), opaques (dark) and quartz (gray or white interference colours) embedded in a microcrystalline matrix (dahllite and quartz exhibit gray or white interference colours). Framboidal pyrite scattered in the collophane. Collophane is corroded and replaced by dahllite. Dahllite is growing at the expense of collophane. Note, cross section from bony vertebrae of fish skeleton was replaced by collophane. Phosphorite, C.N. X40

Nichols (Figs. 4, 6, 8 and 10). The microcrystalline dahllite of the matrix corrodes and replaces the cellophane (Abou El-Anwar et al. 2020), hence the dahllite is growing at the expense of the collophane (Figs. 3, 4, 5, 6, 7, 8, 9 and 10). It also commonly observed that collophane replaces biophases "bone fragments, spines and teeth of vertebrates such

as shark fish as well as coprolites" (Figs. 5, 6, 7 and 8) (Abou El-Anwar and Sadek 2008; Abou El-Anwar et al. 2020).

Dahllite ($3Ca_3(PO_4)_2 \cdot CaCO_3$) was microscopically recorded for the first time in the phosphorite at (Duwi Formation) in Qusier-Safaga area, Central Eastern Desert, Egypt (Abou El-Anwar et al. 2019a, 2020). In the present

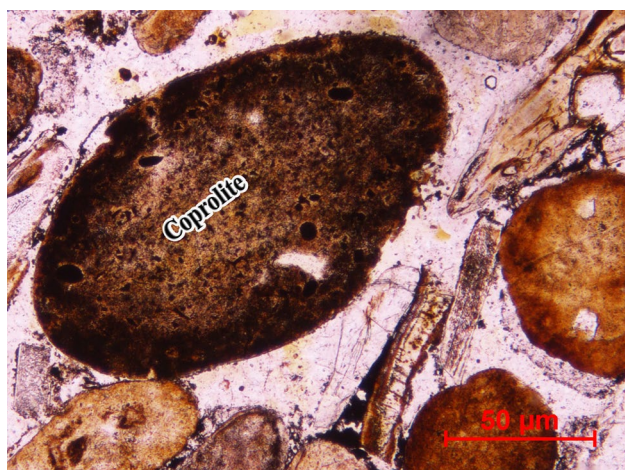


Fig. 9 Photomicrograph showing collophane (brown grains, pellets, spheroids, ovoids) and coprolite (brown cylindrical form) embedded in a microcrystalline matrix (colourless dahllite and quartz). Framboidal pyrite scattered in the collophane. Collophane is corroded and replaced by dahllite. Dahllite is growing at the expense of collophane. Phosphorite, PPL. X40

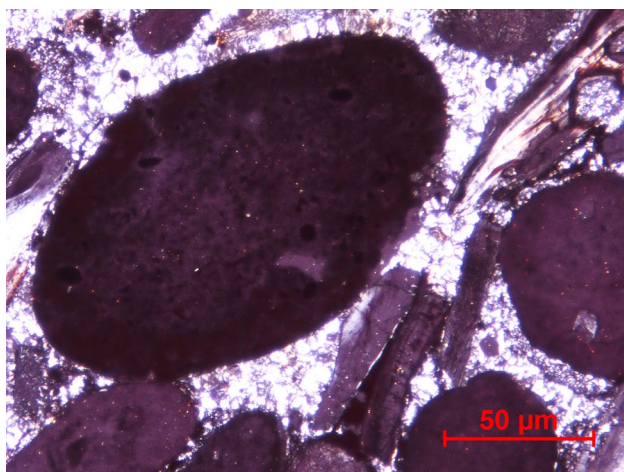


Fig. 10 Photomicrograph showing collophane (isotropic grains, pellets, spheroids, ovoids) and coprolite (isotropic cylindrical form) embedded in a microcrystalline matrix (dahllite and quartz exhibit gray or white interference colours). Framboidal pyrite scattered in the collophane. Collophane is corroded and replaced by dahllite. Dahllite is growing at the expense of collophane. Phosphorite, C.N. X40

study, dahllite belongs to the microcrystalline phosphatic matrix only.

Quartz (SiO_2) forms colourless anhedral equigranular crystals. It exhibits gray or white first order of interference colours (Figs. 3, 4, 5, 6, 7, 8, 9 and 10). It exhibits wavy extinction due to strain.

Opagues are mainly represented by pyrite. It forms subhedral to anhedral grains. It is later oxidized to hematite. Framboidal pyrite is also commonly observed in the form

of framboids that scattered in the collophane (Figs. 7, 8, 9 and 10). Framboidal pyrite is suggesting anoxic conditions and indicating the function of the anaerobic bacteria during early diagenetic stages (Schieber and Baird 2001; Abou El-Anwar 2017; Abou El-Anwar et al. 2019a, 2020).

Mineralogy

The mineralogical composition was recognized by X-Ray Diffraction technique which is represented by two main mineral phases in the studied phosphatic rocks of Um El-Huwat samples. Phosphatic phase represented by apatite (fluorapatite) which is the dominant (Fig. 11). Occurrence of francolites is revealing that the phosphatic rocks have significant quantities of carbonates. On the other side, the non-phosphate minerals include carbonate minerals; calcite, dolomite, evaporated mineral (gypsum), sulphide mineral (pyrite), in addition to quartz as a silicate mineral. These results are confirmed by XRD analysis.

SEM and EDX examination of the phosphatic samples was showing the dominance of the bone fragments, halite crystals and quartz grains scattered in the matrix (Fig. 12), EDX recorded P (15.9%), Ca (29.73%), and Na (4.2%). Framboidal pyrite as authigenic origin, halite crystals and quartz grains are scattered in the matrix (Fig. 13), EDX recorded Fe (5.11%), Si (15.9%), Na (3.37%), and Cl (4.5%). Framboidal pyrite is dispersed in irregular masses and clusters, which is confirmed with XRD analysis. The framboidal pyrite indicated anoxic environment through the early diagenetic stages (Schieber and Baird 2001; Abou El-Anwar and El-Sayed 2008; Abou El-Anwar 2011; 2012, 2014; Abou El-Anwar et al. 2017 and 2020). The presence of pyrite spheres marked possibly shallow marine water (Schieber and Baird 2001; Abou El-Anwar 2020). Pyrite can be oxidized and changed to a ferruginous component during the weathering, which indicates the function of the chemical weathering. Therefore, the Duwi Formation seems to be considerably affected by the chemical weathering, which is in agreement with Abou El-Anwar (2016), Abou El-Anwar et al. (2014),

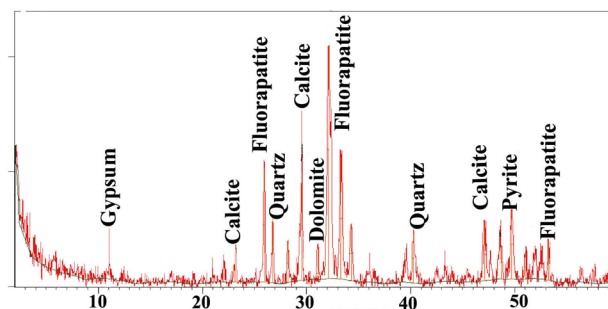


Fig. 11 X-Ray diffractograms for the phosphatic rocks of the studied mine

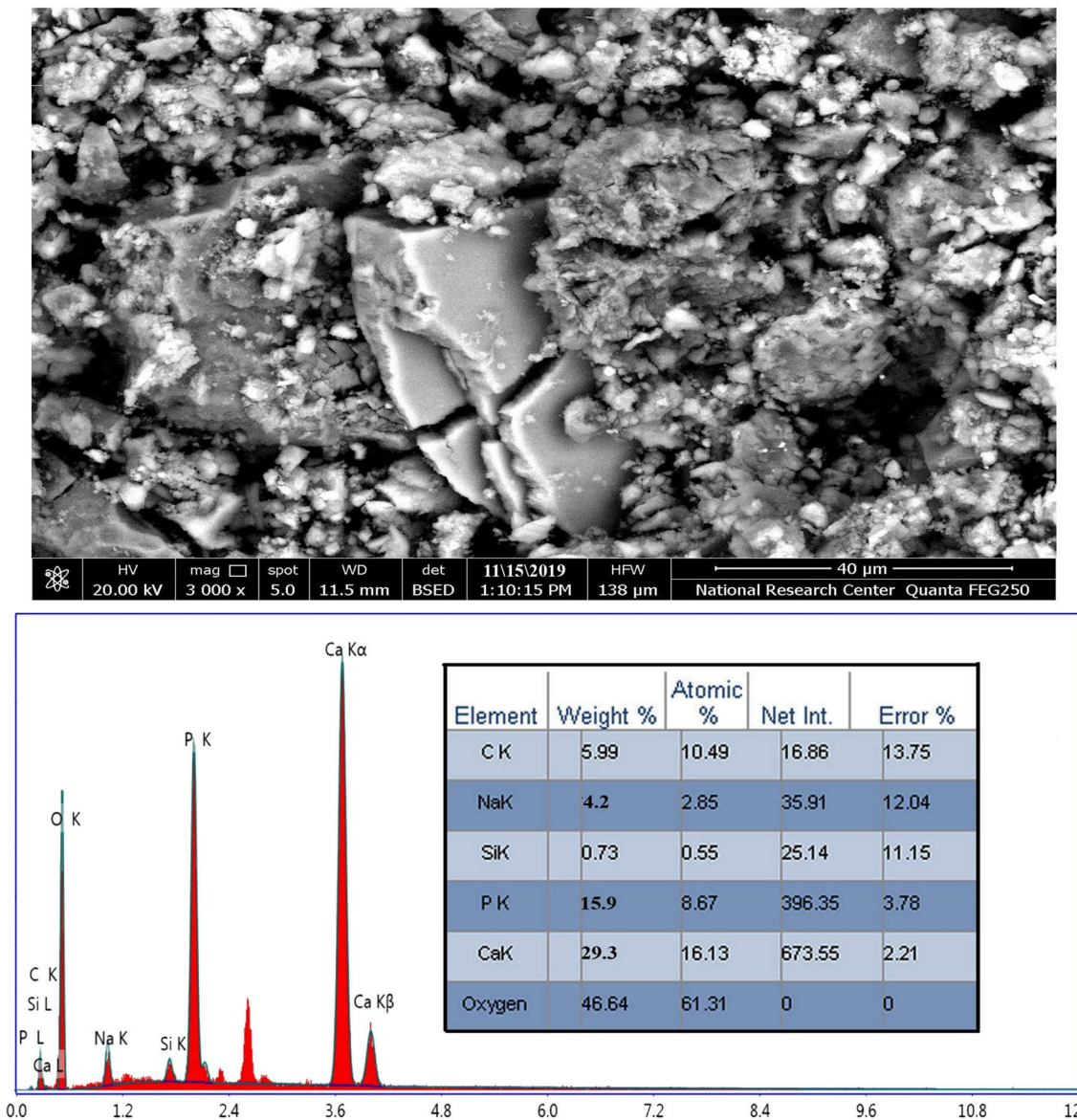


Fig. 12 BSE image and EDX analysis data showing a dominance of the bone fragments, halite crystals and quartz grains scattered in the matrix (Fig. 4), EDX recorded P (15.9%), Ca (29.73%) and Na (4.2%)

Abou El-Anwar et al. (2017, 2019b) and Abou El-Anwar et al. (2020).

Geochemistry

The results of geochemical composition of the major, trace and rare earth elements for the studied phosphatic rocks within the Um El-Huwat mines, along with their ratios are quoted in (Table 1). The interrelationships between elements are shown in (Table 2). The major and trace elemental compositions of the phosphatic rocks in these study region are

compared with the published averages phosphatic rocks in Table 3.

Major elements

Generally, CaO is the dominant constituent of the studied samples ranging from 40.45 to 44.14%, averaging 41.99% (Table 1). P₂O₅ is the second abundant element in abundance. It varies from 25.8 to 29.8% and averaging 27.31%, which indicates the presence of the apatite mineral, as confirmed by the XRD. The moderate positive relation ($r=0.52$) between CaO and P₂O₅, indicated that CaO associated with

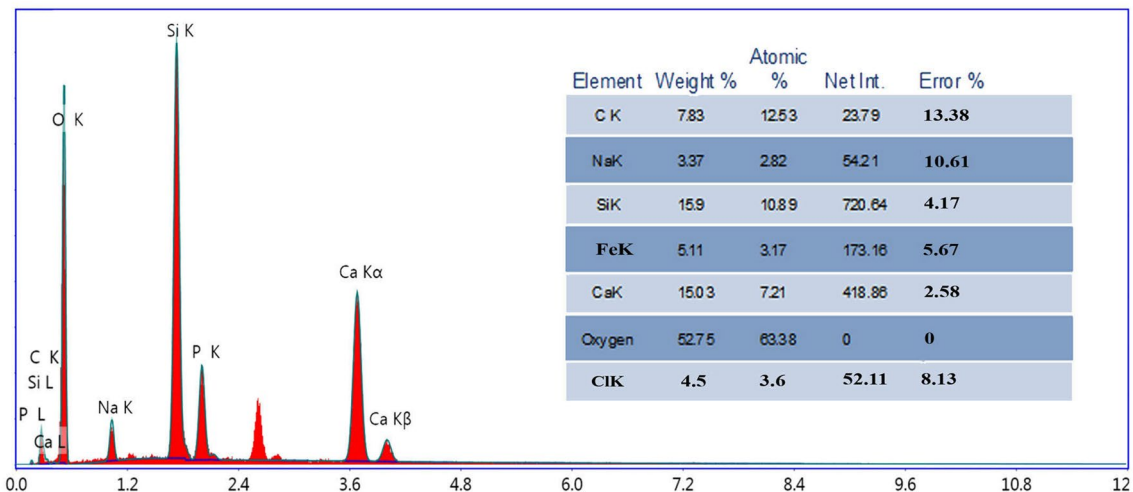
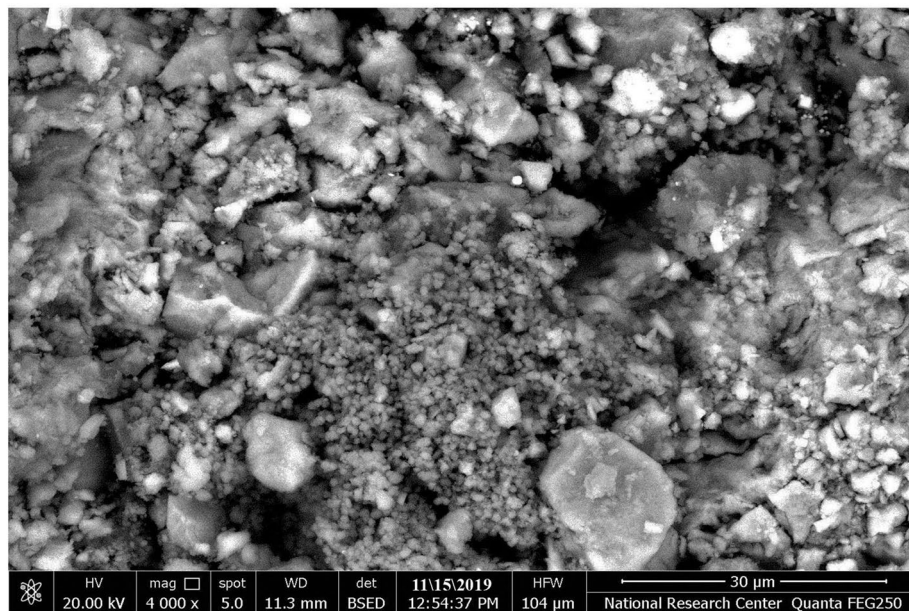


Fig. 13 SEM photograph showing spheres of framboidal pyrite as authigenic origin, halite crystals and quartz grains embedded in the matrix, EDX recorded Fe (5.11%), Si (15.9%), Na (3.37%) and Cl (4.5%)

P_2O_5 as apatite phase as well as there is another phase of CaO represented by calcite mineral, which is confirmed by the XRD (Table 2 and Fig. 11). The average of MgO was 1.13%, and the strong positive correlation ($r=0.67$) between Ca and MgO was revealed that the studied samples have dolomite mineral (Table 2), which is confirmed by the XRD.

Phosphate rocks at Um El-Huwat are classified as high-grade ore (26–35% P_2O_5) according to (Ozer et al. 2000; Sengul et al. 2006). More than 20% of P_2O_5 indicates the dominance of the apatite group minerals, such as hydroxyl-fluorapatite, carbonate fluorapatite. Therefore, the composition of the studied phosphatic rocks (averaging $P_2O_5=27.31\%$) is mainly fluorapatite as confirmed by the XRD results. The average CaO/ P_2O_5 for Um El-Huwat

phosphatic rocks is (1.54) as showing in (Table 1); hence, they are relatively comparable to the pure fluorapatite (1.317).

SO_3 represent the third element in abundance, which ranges from 6.41 to 10.40% with averaging 8.79%. Fe_2O_3 up to 3.44% and average 2.75%, the strong positive correlation ($r=0.70$) between Fe_2O_3 and SO_3 indicated the presence of pyrite mineral (cf. Xiugen et al. 2010; Abou El-Anwar 2017; Abou El-Anwar et al. 2017, 2019b, 2020), which is confirmed by the XRD, SEM and petrographic analysis. SiO_2 contents up to 5.1% and average 4.52%. Al, Na, K, Ti and F are recorded in low percentages. The positive correlation between Al_2O_3 with both SiO_2 and NaO ($r=0.64$ and 0.34, respectively), revealed the presence of some clay minerals.

Table 1 XRF data major (%), trace and rare earth elements (ppm), elemental ratios and CIA of selected studied samples in the phosphatic rocks of Um El-Huwat mine

Element	1	2	3	4	5	6	7	Min	Max	Average	EF
P ₂ O ₅	29.8	26.25	25.8	27.14	26.18	27.89	28.12	25.8	29.8	27.31	182.08
SiO ₂	4.45	4.67	4.6	4.15	5.1	4.09	4.61	4.09	5.1	4.52	0.07
Al ₂ O ₃	0.32	0.38	0.36	0.41	0.54	0.37	0.42	0.32	0.54	0.4	0.03
TiO ₂	0.07	0.03	0.03	0.03	0.03	0.04	0.03	0.03	0.07	0.04	0.06
CaO	44.14	42.31	41.12	40.45	42.68	41.11	42.15	40.45	44.14	41.99	11.7
MgO	1.64	0.96	1.31	0.81	1.14	1.12	0.96	0.81	1.64	1.13	0.42
Fe ₂ O ₃	1.02	3.68	2.81	1.24	2.68	3.94	3.9	1.02	3.94	2.75	0.55
Na ₂ O	0.51	1.3	1.12	1.11	1.04	1.04	1.03	0.51	1.3	1.02	0.31
K ₂ O	0.13	0.07	0.07	0.06	0.07	0.07	0.06	0.06	0.13	0.08	0.03
SO ₃	6.41	10.18	7.18	8.15	10.4	10.12	9.1	6.41	10.4	8.79	56.69
F	1.03	0.88	0.88	0.78	0.57	0.64	0.67	0.57	1.03	0.78	14
Cl	0.11	0.75	0.75	0.71	0.54	0.64	0.45	0.11	0.75	0.56	15.14
L.O.I	10.37	8.54	8.97	14.96	9.03	8.93	8.5	8.5	14.96	9.9	–
Mn	835	210	450	750	551	610	810	210	835	602.29	0.78
Sr	2310	1231	1271	450	920	1645	2104	450	2310	1418.71	4.43
Ba	114	80	44	61	81	95	66	44	114	77.29	0.12
Co	44	39	31	41	35	42	43	31	44	39.29	2.27
Cr	361	310	290	341	305	344	351	290	361	328.86	3.57
Cu	91	71	55	88	69	75	89	55	91	76.86	2.74
Ni	430	143	142	135	120	241	324	120	430	219.29	4.67
Pb	320	280	240	300	245	308	310	240	320	286.14	550.27
Mo	92	75	59	89	66	88	90	59	92	79.86	72.6
Zn	410	320	310	329	311	340	390	310	410	344.29	5.14
V	1300	810	510	940	925	1241	1320	510	1320	1006.57	10.94
As	32	24	20	32	29	30	41	20	41	29.71	6.19
Cd	30	22	19	25	22	24	27	19	30	24.14	268.25
Zr	57	62	50	35	64	41	54	35	64	51.86	0.27
La	30	25	20	28	22	26	27	20	30	25.43	0.67
Ga	22	25	23	15	28	23	20	15	28	22.29	1.27
Nb	17	12	13	14	13	14	13	12	17	13.71	1.14
Nd	6	3	1	5	4	5	5	1	6	4.14	0.15
Sc	21	14	15	19	15	18	20	14	21	17.43	1.24
Se	43	24	18	30	20	27	92	18	92	36.29	403.17
Rb	85	99	90	80	105	75	85	75	105	88.43	1.05
Y	25	28	27	22	38	20	33	20	38	27.57	1.31
Ru	12	3	6	4	3	4	5	3	12	5.29	15.55
Bi	3	1	1	2	1	2	3	1	3	1.86	11.61
U	152	120	90	122	111	140	133	90	152	124	44.29
Uc	72.88	62.22	62.02	67.08	75.3	79.89	80.29	62.02	80.29	71.38	–
Th	1.2	1.5	1.2	0.9	1.8	0.8	1.6	0.8	1.8	1.29	0.12
V/MO	14.13	10.8	8.64	10.56	14.02	14.1	14.67	8.64	14.67	12.42	–
V/Ni	3.02	5.66	3.59	6.96	7.71	5.15	4.07	4.25	3.07	4.59	–
V/(V + Ni)	0.75	0.85	0.78	0.87	0.89	0.84	0.8	0.81	0.75	0.82	–
V/(V + Cr)	0.78	0.72	0.64	0.73	0.75	0.78	0.79	0.64	0.79	0.75	–
Mo/U	0.61	0.63	0.66	0.73	0.59	0.63	0.68	0.66	0.61	0.64	–
U/Mo	1.65	1.6	1.53	1.37	1.68	1.59	1.48	1.53	1.65	1.55	–
Rb/Sr	0.04	0.08	0.07	0.18	0.11	0.05	0.04	0.17	0.05	0.06	–
V/Cr	3.6	2.61	1.76	2.76	3.03	3.61	3.76	1.76	3.66	3.06	–
U/Th	126.67	80	75	135.56	61.67	175	83.13	112.5	84.44	96.44	–
Th/U	0.01	0.01	0.01	0.01	0.02	0.01	0.01	0.01	0.01	0.01	–
	14.57										

Table 1 (continued)

Element	1	2	3	4	5	6	7	Min	Max	Average	EF
Fe/Ti		122.67	93.67	41.33	89.33	98.5	130	14.57	130	84.3	–
CIA	21.77	12.46	13.48	15.24	20.07	14.68	16.54	12.46	21.77	16.32	–
Σtrace	3167	2156	1726	2355	2191	2774	3039	1689	3203	2486.86	–
ΣREE	536.2	463.5	394.2	433.9	476.8	449.8	559.6	343.8	640.8	473.4	–
ΣLREE	69	62	56	57	63	63	60	47	75	61.4	–
ΣHREE	25	28	27	22	38	20	33	20	38	27.6	–
ΣLREE/ΣHREE	2.76	2.21	2.07	2.59	1.66	3.15	1.82	2.35	1.97	2.23	–
Nio/Co	9.77	3.67	4.58	3.29	3.43	5.74	7.53	3.87	9.77	5.58	–

Strong positive correlation ($r=0.94$) between Na and Cl, indicated the presence of halite, which is confirmed by the SEM analysis.

Generally, the concentrations of the most common major elements CaO, P₂O₅, SO₃ and Fe₂O₃ (41.99, 27.31, 8.79 and 2.75%, respectively) in the studied samples are higher than those of the same mine (35.57, 25.75, 6.95 and 1.37%) studied by Abou El-Anwar et al. (2019b). Except, Al₂O₃ contents (5.87%) recorded by Abou El-Anwar et al. (2019b) was higher than this measured in the present study samples.

Trace and rare earth elements

The enrichment of the trace and rare earth elements in sediments may be resulting from sea water, hydrothermal or diagenesis. The average trace and rare earth elements content; Sr, V, Cr, Pd, Zn, Ni, U, Mo, Cu, Co, Se, As, Y, Cd, Ga, Sc, Ru and Bi in Um El-Huwat phosphate samples (1419, 1007, 329, 286, 241, 219, 124, 80, 77, 39, 36, 30, 28, 24, 22, 17, 5 and 2 ppm, respectively) are enriched than those in the UCC and PAAS (Taylor and McLennan 1985; Rudnick and Gao 2014, respectively), (Table 1 and Fig. 14). Generally, the studied Um El-Huwat phosphatic samples are enriched in all elements except Ba, Y and Bi than those for the same locality studied by Abou El-Anwar et al. (2019b).

REE compositions of the phosphatic rocks have been modeled formerly to assess the mechanism of REE uptake and subsequent alteration during diagenesis (Chen et al. 2015; Zhang et al. 2016) and recognize the palaeo-seawater REE compositions (Lécuyer et al. 2004; Abbott et al. 2015). Thus, REE associated with phosphatic rocks can be attributed to either adsorption or substitution procedure during diagenesis (Kohn and Moses 2013), and/or subjected to the intensive chemical weathering (Abou El-Anwar et al. 2019b).

P₂O₅ has very strong positive correlation with the most heavy metals Cr, Co, Cu, Ni, Pb, Zn, Mo and V, ($r=0.93$, 0.85, 0.81, 0.94, 0.87, 0.94, 0.84 and 0.86, respectively, (Table 2), and with rare earth elements La, Nb, Nd, Sc, Se, Ru, Bi and U ($r=0.86$, 0.84, 0.83, 0.90, 0.53, 0.75, 0.92 and 0.92, respectively, Table 2). Thus, it indicates that these trace

and rare earth elements are mostly associated with phosphatic rocks. SiO₂ has positive correlation with, Zr, Ga, Rb, Y and Th ($r=0.87$, 0.72, 0.93, 0.94 and 0.94, respectively) which revealed that these elements may be coupled with the detrital quartz.

These trace and rare earth elements are positively correlated with TiO₂ and with each other, which revealed that these elements may be associated with titanium-iron oxides or with the heavy minerals rather than with apatite (Table 2), (cf. Abou El-Anwar and Samy 2013; Abou El Anwar 2019). In addition, the moderate positive correlation ($r=0.45$, 0.33, 0.33 and 0.21, respectively) between S and La, Y, Th and Zr, revealed that pyrite also can be considered as another possible source for REEs (Deditius et al. 2011; Khorasanipour and Jafari 2018).

Distribution of Uranium and Thorium

U content in the studied samples are ranges from 90 to 152 ppm and average 124 ppm from the studied Um El-Huwat phosphatic rocks (Table 1). These values are higher than U content in the UCC (2.5 ppm) and the PAAS (2.7 ppm), (Taylor and McLennan 1985; Rudnick and Gao 2014, respectively). U average content is higher than which is recorded in the same locality studied by Abou El Anwar et al. (2019b). This could be attributed to the post-depositional enrichment of uranium and/or intensive chemical weathering in Quseir area.

Table 2 show that U has strong positive correlation with P₂O₅ and moderate positive correlation with CaO and Sr ($r=0.92$, 0.47 and 0.62, respectively), which indicates that uranium was best associated with these elements in phosphate minerals. In addition U has strong positive correlation with Ti ($r=0.70$) which points to that uranium can be associated with titanium oxide minerals.

The strong and moderate ($r=0.92$ and 0.47, respectively) positive correlation of U with P₂O₅ and Ca indicated that the important role of phosphate in fixation of U⁶⁺ as uranyl ion (UO₂)²⁺. Thus, the secondary uranium minerals such as phosphuranylite {Ca (UO₂) (PO₄)₂(OH)₂6H₂O} may be precipitated. The positive correlation ($r=0.47$) between CaO

Table 3 The trace elemental composition of the phosphates in this study as compared with published average phosphates in different countries

Element	Study area	Yunis	UM El-Huwat, 2019	Tunisia	Morocco	Jordan	AWP	ASC	Soil EC	Fertilizer
Ni	219.29	207	178	55	41.4	15	53	68	50	180
Zn	344.29	159	332	226	279	121	195	95	200	1850
Sr	1418.71	896	1463	1606	1331	n.d	1900	300	n.d	n.d
V	1006.57	1626	365	n.d	n.d	n.d	n.d	n.d	n.d	n.d
Cr	328.86	767	310	42.7	217	51	125	90	60	n.d
Co	39.29	0	185	0.3	0.75	n.d	7	19	n.d	150
Mo	79.86	365	0	14.1	7.9	n.d	n.d	2.5	n.d	20
As	29.71	70	24	11	10.7	n.d	23	13	8	75
Mn	602.29	958	492	51.2	15	n.d	n.d	850	n.d	n.d
U	124	50	97	40	n.d	n.d	n.d	n.d	n.d	n.d

Tunisia, Morocco, (Silva et al. 2010); Jordan (Batarseh and El-Hasan (2009); AWP (Altschuler 1980); ASC: Average Shale Composition by Turekian and Wedepohl (1961); Soil EC: (European Commission EC 1986), Fertilizer Canada: Permissible limit established by the Canadian Food Inspection Agency (1997). *n.d.* not determined

and U indicated that part of the U content may be occurs as tetravalent state U^{4+} resulting of substitution for Ca^{2+} in the phosphate minerals during subaerial weathering (Abou El Anwar et al. 2019b). Also, the strong positive ($r=0.73$) correlation between P_2O_5 with Sr is may be probably interrelated to the occurrence of belovite $\{Sr_3(CeNaCa)_2(PO_4)_3OH\}$ mineral. Thus, phosphuranylite and belovite may be deposited in the study area as secondary minerals which are in agreement with Abou El Anwar et al. (2019b).

U is strong positive correlated with Co, Cr, Cu, Ni, Pd, Mo, Zn, V, As, Cd, La, Nb, Nd, Sc and Bi ($r=0.95, 0.92, 0.82, 0.80, 0.92, 0.90, 0.81, 0.93, 0.65, 0.90, 0.90, 0.67, 0.91, 0.77$ and 0.80 , respectively). Therefore, U may be released during the weathering and behave as immobile and it can be change to a new phases (Venter and Boylett 2009). Thus, U contents in the study phosphatic rocks were probably associated with the heavy metals and rare earth elements during the chemical weathering (Waite et al. 1994; Bots and Behrends 2008; Bata 2016; Abou El-Anwar 2019; Abou El-Anwar et al. 2020) under oxic environment (Song et al. 2012). Thus, anoxic sediments are much more enriched in U than oxic ones (Wignall and Twitchett 1996; Abou El-Anwar 2019; Abou El-Anwar et al. 2020).

The geochemistry of Mardin-Mazidag Phosphate Deposit (Akuze et al. 2008) which was studied using the quadratic regression model of Narula and Wellington (2007). This quadratic regression used to illustrate comparatively wide area of the input variable changes. It is expressed as follows:

$$Y = b_0 + \sum b_i x_i + \sum b_i x_i^2, \quad (1)$$

where Y represents the U concentration in ppm and X_1, X_2 represent P_2O_5 and F concentration in %, respectively. These parameters used to explain the relation between Phosphate,

Fluorite and Uranium. After the regression analysis for them experiment, the following mathematical model was obtained:

$$Y = -8.9614 + 3.0972X_1 - 10.1493X_2.$$

As a result, the interrelation between P_2O_5 , F and U concentrations of the phosphate ore samples could be expressed as follows:

$$U_{(mg/kg)} = -8.9614 + 3.0972 P_2O_{5(st.\%)} - 10.1493 F_{(wt.\%)}. \quad (2)$$

The calculated U (mg/kg) for Um El-Huwat which is shown in Table 1.

Thus, the studied Um El-Huwat phosphatic samples have high P_2O_5 and low organic matter. The U_m have high value versus to the U_c , which support that anoxic sediments are much more enriched in U in Um El-Huwat phosphates mines.

The values of the studied samples are higher than U_c values; this could be attributed to the post-depositional enrichment of uranium and/or the intensive chemical weathering.

In contrast, the studied samples recorded Th which is not detected by Abou El-Anwar et al. (2019b). Th content varies from 0.8 to 1.8 ppm with averaging 1.29 ppm in the present study; this value was lower than those recorded in UCC (10.3 ppm) and PAAS (10.5 ppm), (Taylor and McLennan 1985; Rudnick and Gao 2014, respectively). Th is strong positive correlated ($r=0.94$) with SiO_2 and moderately with Al_2O_3 ($r=0.62$), which indicates that the Th content is mainly associated with quartz and clay minerals. Also, it is weak positive correlated with Fe_2O_3 and SO_3 , which reveals that the Th possibly weak coupled with pyrite mineral. Th is strong positive correlated ($r=0.87$) with the trace element Zr, in addition it is strong to moderated positive relation with

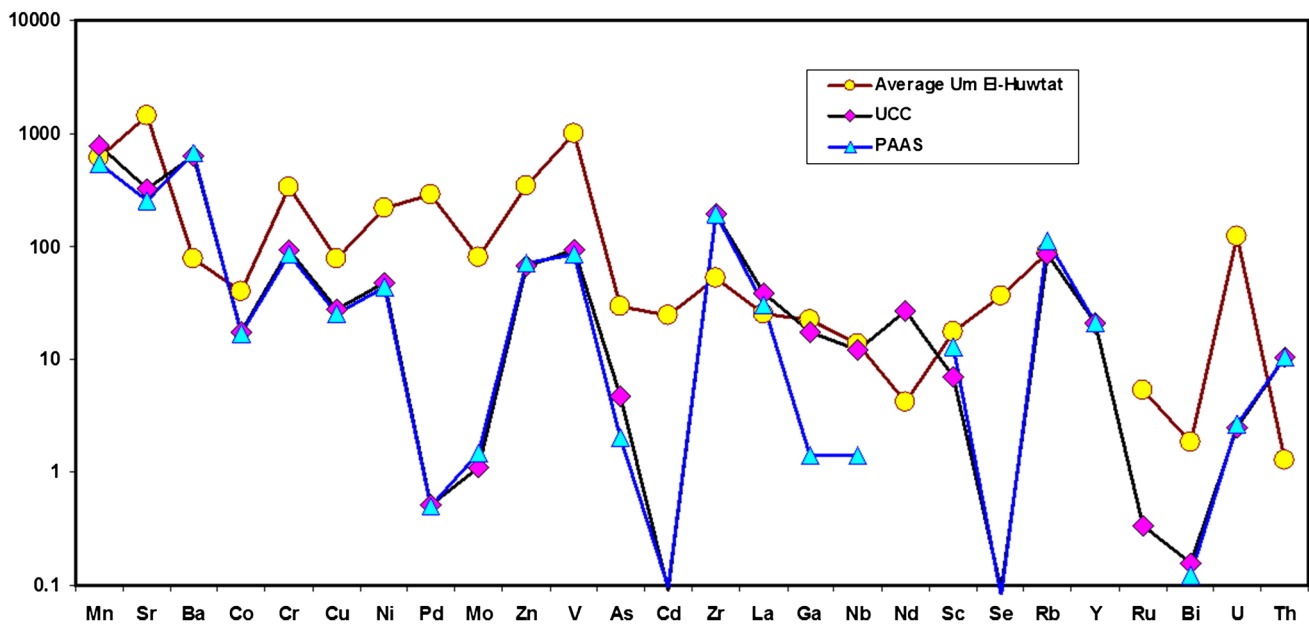


Fig. 14 Concentrations of the trace and rare earth elements in the studied phosphatic rocks normalized by UCC and PAAS

some rare earth elements; Y, Rb and Ga ($r=0.96$, 0.85 and 0.58 , respectively). Zr is strong positive correlated ($r=0.77$, 0.84 and 0.78 , respectively) with the rare earth elements Y, Rb and Ga. Thus, Th probably associated with zirconium mineral and its rare earth associated in the detrital quartz.

Depositional environment

V, Ni, Mo, U, Cu, Cr, Re, Cd, Sb and Tl are represented by redox-sensitive trace elements in marine sediments. Thus, they can point to the paleo-conditions (Pattan and Pearce 2009; Adegoke et al. 2014; Pi et al. 2014). The redox-sensitive metals are highly enriched in anoxic sediments.

The average redox-sensitive trace elements (V, Ni, Mo, U, Cu, Cr, Cd, Co and Zn) in the studied phosphatic rocks from the Um El-Huwat mine (1007, 219, 80, 124, 77, 329, 24, 39 and 242 ppm, respectively) show enrichments of the redox-sensitive elements (97, 47, 1.5, 2.5, 28, 92, 0.098, 17.3 and 67 ppm, respectively) compared to the composition of the bulk continental crust (Rudnick and Gao 2014; Fig. 14). This enrichment in the contents of the redox-sensitive elements of the Um El-Huwat phosphatic rocks can be pointed out to a strong evidence for anoxic environment through the deposition (Pi et al. 2014; Adegoke et al. 2014). This is in agreements with Abou El-Anwar (2016, 2017), Abou El-Anwar et al. (2017, 2019b, 2020). The more enrichment of the most trace and rare earth elements were may be probably resulting of they were leached from the above Dakhla shales in the study area. V is enriched in comparison to Ni in anoxic marine environments which may be due to the strong activity of sulfate reducing bacteria in this environment in

addition to V is comparatively higher stability compared to Ni (Peters and Moldowan 1993).

V/Mo ratio in sediments < 2 , it indicates an anoxic condition, ratio between 2 and 10 indicates suboxic conditions, and it from 10 to 60 indicates oxic conditions (Gallego-Torres et al. 2010).

V/Ni ratio higher than 3 indicates that marine origin organic matter was deposited under reducing conditions (Galarraga et al. 2008).

V/(V + Ni) and V/(V + Cr) ratios can be used to indicate oxygenation of the depositional environment, and higher V/(V + Ni) and V/(V + Cr) ratios indicate more strongly reducing conditions. Pi et al. (2014) recognized V/(V + Ni) and V/(V + Cr) ratios of more than 0.8 and 0.6, respectively, to indicate strongly reducing conditions. V/Cr > 4.25 denoting an anoxic environment and from 2.0 to 4.25 indicates a suboxic to dysoxic environment. Ni/Co > 7.0 indicate anoxic, from 5.0 to 7.0 declares suboxic to dysoxic and lower than 5.0 point to oxic environment (Jones and Manning 1994; Shi et al. 2015).

V/Mo ratio in the studied phosphatic samples ranges from 8.6 to 14.7 averaging 12.42 indicated to oxic conditions of deposition (Table 1). The Um El-Huwat phosphatic samples recorded V/Ni ratio (4.59) indicated that the deposition took place under anoxic reducing conditions, (Galarraga et al. 2008; Table 1).

V/(V + Ni) and V/(V + Cr) ratios recorded 0.82 and 0.75, respectively. Thus, the studied samples from Um El-Huwat phosphatic rocks are display more reducing nature of their depositional environment (Table 1).

V/Cr (3.06) higher than 2.0 (Table 1), this indicate that the phosphatic rocks in the studied area in the stage of late stage diagenesis (Trueman and Tuross 2002), which confirmed by the mineralogically and petrographically studied. In the studied phosphatic samples the V/Cr (3.06) indicates that these phosphatic rocks are deposited under suboxic to dysoxic environment (Jones and Manning 1994). Ni/Co ranging from 3.87 to 9.77 revealed that the deposition of the studied phosphatic samples in oxic to anoxic condition.

U/Th > 1.25 indicates an anoxic environment, and 0.75–1.25 sign a suboxic to dysoxic environment, while a < 0.75 indicates an oxic environment (Jones and Manning 1994; Shi et al. 2015). U/Th (96.4) indicated that the studied rocks were deposited in anoxic condition. Th/U was recorded 0.01 indicates mainly anoxic environment (Pi et al. 2014).

U content higher than 12 indicates anoxic conditions, range from 5 to 12.0 indicates suboxic to dysoxic conditions, while the < 5.0 indicates oxic conditions. The studied area recorded average 124 ppm U. Thus, it was deposited under anoxic conditions (Algeo and Tribovillard 2009).

Fe/Ti for the study shales is 84.30, which is consistent with hydrothermal input as well (Delian et al. 2004). Consequently, the studied black shales most probably resulted from mineralization by the hydrothermal solution, which is in agreement (Abou El-Anwar et al. 2019b, 2020).

Consequently, the trace elements and the ratio of V/Mo, V/Ni, V/Cr, V/(V + Ni), and V/(V + Cr), Ni/Co, U/Th, Th/U and authigenic uranium as well as Fe/Ti can be indicate the redox conditions of rocks and the results declare the oxic to anoxic environment coupled with hydrothermal solution in the studied phosphatic rocks are deposited (cf. Abou El-Anwar et al. 2018, 2019b).

Mobilization of rare earth elements

Generally, REEs are mainly originated from rock and mineral weathering, erosion and soil parent material (Jiang and Ji 2012). Concentrations of REEs naturally found in sediments depend on the parent material.

Table 1 reveals that LREE (61.4 ppm) enrichment and HREE (27.6 ppm) depletion, which indicated that the consequence of the weathering process. The LREE/HREE ratios (2.23) showed that weathering processes had an impact on REE fractionation in the studied area. Resulting of the lower mobility of LREE compared with HREE indicated to the LREE enrichment, whereas HREE depletion accompanying with increase weathering strength (Yusoff et al. 2013; Gao et al. 2016). Generally, the intensity of weathering environments led to raise the ratio of LREEs/HREEs in sediments derived from metaluminous granites (Yusoff et al. 2013).

Data analysis in Table 2 indicated that most LREEs (La and Nd) are mainly strong positive correlated with P

($r = 0.86$ and 0.83 , respectively) and Ga strong positive correlated with Si ($r = 0.72$), which indicated that the most LREEs are associated with phosphatic samples and few associated quartz grains. Whereas, HREE; Y and Sc strong positive relation with Si and P; reservedly ($r = 0.94$ and 0.90 , respectively) which revealed that the HREE are associated with phosphatic and quartz grains which is more resistant to weathering, which is in agreements with Caspari (2006). Generally, REEs have minimum mobility within near-surface environments. Thus, these minerals those reflect nearby sources.

Enrichment factor EF

The trace elements Pb, Se, Cd, Mo, Th, Ru, U, V, As, Zn, Ni, Sr, Cr, Cu and Co are enriched with enrichment values (EF) of 550.27, 403.1, 268.25, 72.6, 44.3, 15.5, 11.6, 10.9, 6.16, 5.14, 4.67, 4.43, 3.57, 2.74 and 2.27, respectively. The enrichment of these elements is consistent with high organic matter content and abundant pyrite crystal found in phosphate samples because they are hosted in sulphides and/or organic associated (Spear and Zheng 1999). The elements Y, Ga, Nb, Nd, Sc, Mn, Rb and La, Cu, Ni and Th have enrichment values 1.31 to 1.05 which is understandable because they are probably controlled by sulphides and /or organic matter, (Eskenazy 2009). Zr, Ba and Nd have an EF less than 0.5 and are thus considered to be depleted. The depletion of these elements is possibly attributed to weathering source rocks because they are mainly or partly present in clay minerals. All other elements studied show more or less the same concentration as the Clarke values with the EF between 1.3 and 0.5. Obviously, the enrichment or deletion of an element may be a function of that association and the origins of the various phosphate fractions.

Paleoclimate

The CIA can be reflecting the paleoclimatic conditions. CIA from 50 to 65, indicated cold and dry climate during low chemical weathering, 65 to 85, it denotes a warm and humid climate during moderate chemical weathering, while a value between 85 and 100 indicated a hot and humid climate during strong chemical weathering (Nesbitt and Young 1982; McLennan 1993). The CIA of the studied phosphatic rocks is ranged between 12.46 and 21.77 with averaging 16.32% indicating that these rocks were subjected low intensive chemical weathering condition (Fedot et al. 1996). The immobile elements can be used as markers of provenance such as weathering (Taylor and McLennan 1985). Thus, the strong positive and Ni, Zn, V, Zr, Cr, Rb, Y and U ($r = 0.82$, 0.55, 0.81, 0.81, 0.62, 0.86, 0.64 and correlations between Al_2O_3 0.54, respectively, Table 2) as well as moderate

relation with Cd and La ($r=0.33$ and 0.15 , respectively) reveal that these immobile elements are concentrated during weathering processes (Fedó et al. 1996).

Rb/Sr ratios can be used to identify the degree of source rock weathering (McLennan 1993). The studied shale samples have an average Rb/Sr ratio of 0.06 (Table 1). This value is lower than that of the UCC average (0.33) and is relatively comparable to PAAS (0.08). This suggests that the degree of the chemical weathering of the source rocks was relatively comparable to the PAAS values.

Comparison of the chemical composition with published averages of other contraries:

Table 3 shows the distribution of the trace and rare earth elements in the study phosphatic rocks and in other different localities. The phosphatic rocks in Quseir area are enrichment in V, Zn, Cr, Mo, Mn, Ni, Co, As and U than all the other contraries (Table 3 and Fig. 16). Yunis phosphatic samples were high contents in V, Cr, Mo, As and Mn, (Abou El-Anwar et al. 2019b) than the studied phosphatic rocks. In addition the studied samples rich in all the elements except Sr, Co and U than those detrained by (Abou El-Anwar et al. 2019b) for the same mine (Fig. 15).

Table 3 and Fig. 16 show that all the elements contents are higher than those in Average World Phosphorite (AWP) recorded by Altschuler 1980) except Sr content, and the Fertilization Food (Canadian Food Inspection Agency 1997), except Zn content. Furthermore, all the average values for the elements are higher than those in Average Shale Composition (ASC) and UCC (Turekian and Wedelphl 1961; Rudnick and Gao 2014). Thus, it may be concluded in the Duwi Formation, at Quseir region the phosphatic rocks are suitable for industrialized fertilizers.

The average Ni, Zn, V, Cr, Mo, As, Mn and U content in the study area are higher than those for the same mine which studied with Abou El-Anwar et al. (2019b), except Co is lower (Table 3 and Fig. 16). The average Ni, Zn, Sr, Cr and U content in the study area are higher than those for the phosphatic samples of Yunis mine (Abou El-Anwar et al. 2019b). Also, all the recoded values for the study mine are higher than those in Tunisia, Morocco (de Silva et al. 2010), and Jordan (Batarseh and El-Hasan 2009), except Sr (1606 ppm) content in Tunisia is higher than our samples. Figures 17 and 18 show the distribution of the trace elements Ni, and U average values are higher than those of all localities and other countries.

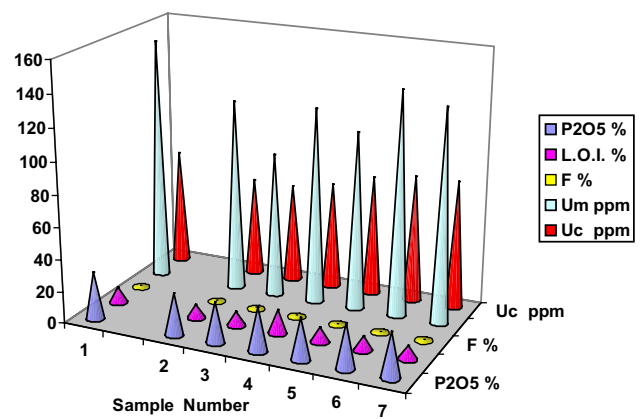


Fig. 15. 3-D pyramids plotting showing the Yunis and Um El-Huwat concentration data series of U.m (measured uranium) in ppm, U.c (calculating uranium) after Akyuz et al. (2008)

Conclusions

Mineralogical, petrographical and geochemical investigations for the phosphate rocks in Um El-Huwat (Safaga) mines of the Duwi Formation at Quseir area are made to recognize the depositional environment. Mineralogically, the bulk samples are mainly apatite (francolites). The non-phosphatic minerals include quartz, calcite, dolomite and pyrite.

The studied phosphatic rocks of the study area are generally having high concentrations of some trace and rare earth elements. They are accumulated under oxic to anoxic condition. High values for Fe/Ti suggests a biogenic and hydrothermal source for the Fe. The intensity of weathering environments led to raise the ratio of LREEs/HREEs. They are accumulated from nearby sources.

In comparison with the Average World Phosphorite (AWP), the Fertilization Food the studied phosphatic rocks are higher in all elements expected Sr (1900 ppm for AWP) and Zn (4850 ppm for Fertilization Food). Thus the studied phosphatic rocks are suitable for industrialized fertilizers according to the world guides. In addition, they have economic values resulting of the enrichment in some traces and rare elements.

All the average values of the heavy metals are higher than those in Tunisia, Morocco and Jordan (400.3, 571.75 and 187 ppm, respectively) for the study mine.

Funding Open access funding provided by The Science, Technology & Innovation Funding Authority (STDF) in cooperation with The Egyptian Knowledge Bank (EKB).

Open Access This article is licensed under a Creative Commons Attribution 4.0 International License, which permits use, sharing, adaptation, distribution and reproduction in any medium or format, as long as you give appropriate credit to the original author(s) and the source,

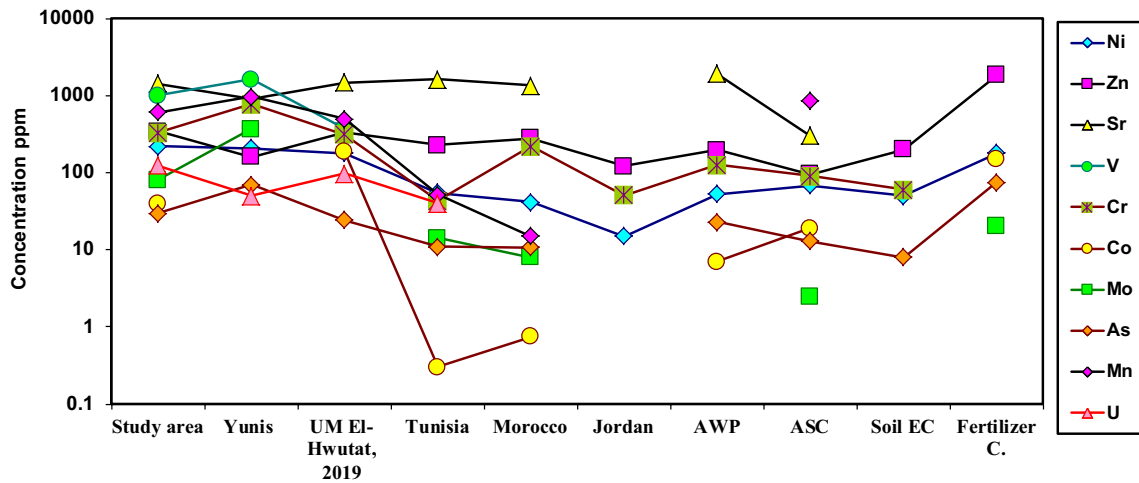


Fig. 16 Distribution the trace elements for the study area and others

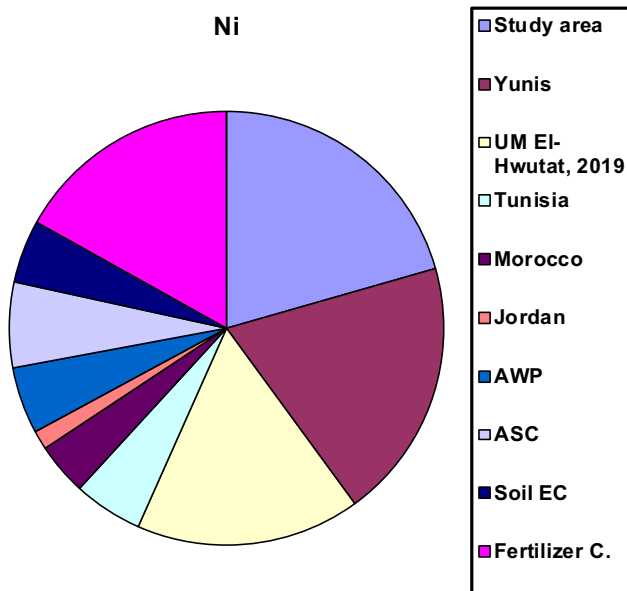


Fig. 17 Pie diagram shows the distribution of Ni for the study mine and others

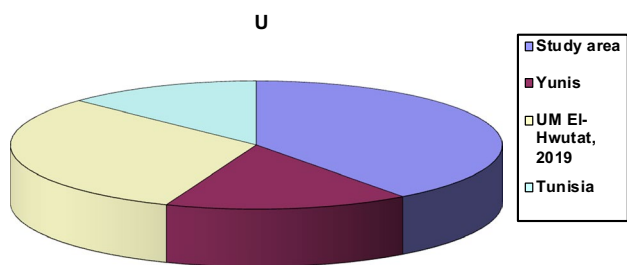


Fig. 18 Pie diagram shows the distribution of U for the study mine and others

provide a link to the Creative Commons licence, and indicate if changes were made. The images or other third party material in this article are included in the article's Creative Commons licence, unless indicated otherwise in a credit line to the material. If material is not included in the article's Creative Commons licence and your intended use is not permitted by statutory regulation or exceeds the permitted use, you will need to obtain permission directly from the copyright holder. To view a copy of this licence, visit <http://creativecommons.org/licenses/by/4.0/>.

References

Abbott AN, Haley BA, McManus J, Reimers CE (2015) The sedimentary flux of dissolved rare earth elements to the ocean. *Geochim Cosmochim Acta* 154:186–200

Abou El-Anwar EA (2011) Petrographical, geochemical and diagenetic studies of the middle Eocene carbonates, Mokattam Formation of darb el-fayium area. (Int Conf on geological sciences and engineering, France Paris Augustus 80:1315–1325

Abou El-Anwar EA (2012) Contribution to the composition and origin of the reef terraces in Ras Mohamed, Sharm El-Sheikh Coast, Southern Sinai, Egypt. *Egypt J Geol* 56:33–48

Abou El-Anwar EA (2014) Composition and origin of the dolostones of um bogma formation lower carboniferous, west central Sinai, Egypt. *Carbonates and Evaporites* 29:129–205. <https://doi.org/10.1007/s13146-014-0188-3>

Abou El-Anwar EA (2016) Mineralogical, petrographical, geochemical, diageneses and provenance of the Cretaceous black shales Duwi Formation at Quseir-Safaga, Red Sea, Egypt. *Egypt J Petroleum* 25:323–332

Abou El-Anwar EA (2017) Mineralogical, petrographical, geochemical, diageneses and provenance of the cretaceous black shale Duwi formation at Quseir-Safaga, Red Sea, Egypt. *Egyptian J Pet* 26:915–926

Abou El-Anwar EA (2019) Lithologic characterization of the phosphorite-bearing Duwi Formation (Campanian), South Esna West Nile Valley, Egypt. *Carbonates and Evaporites* 34:793–805. <https://doi.org/10.1007/s13146-018-0442-1>

Abou El-Anwar EA, Sadek MS (2008) Composition of black shale from Quseir, Red Sea, Egypt with emphasis on the sequential extraction of some metals. *Bull NRC Egypt* 32(5):511–536

- Abou El-Anwar EA, Samy Y (2013) Clay mineralogy and geochemical characterization of Some Quaternary sediments on Giza-Fayyum District, Western side of the Nile Valley, Egypt: relationships to weathering and provenance. *Australian J Appl Sci Res* 9(8):4765–4780
- Abou El-Anwar EA, Mekky HS, Samy YM (2014) Contribution to the mineralogical, geochemical and provenance of the Cretaceous black shales, Duwi Formation, Quseir-Safaga, Red Sea Coast Egypt. *Egypt J Geol* 58:303–322
- Abou El-Anwar EA, Mekky HS, Abdel Wahab W (2018) Geochemistry, mineralogy and depositional environment of black shales of the Duwi Formation Qusseir area, Red Sea coast, Egypt. *Carbonates Evaporites*. <https://doi.org/10.1007/s13146-017-0417-7>
- Abou El-Anwar EA, Abd El-Rahim SH, Mekky HS (2019a) Spherulitic dahllite of Duwi Formation phosphorite. *Carbonates Evaporites* 34:557–562. <https://doi.org/10.1007/s13146-017-0377-y>
- Abou El-Anwar EA, Mekky HS, Abdel Wahab W (2019b) Characterization and depositional environment of P₂O₅-F-U of phosphatic rocks for the Duwi Formation Quseir- Safaga Region Red Sea Coast Egypt. *Egypt J Chem* <https://doi.org/10.21608/ejchem.2019.11366.1728>
- Abou El-Anwar EA, Mekky HS, Abd El Rahim SH, Aita SK (2017) Mineralogical, geochemical characteristics and origin of Late Cretaceous phosphorite in Duwi formation (Geble Duwi Mine) Red Sea region, Egypt. *Egyptian J Pet* 26:157–169
- Abou El-Anwar EA, Mekky HS, Abd El Rahim SH, El-Sankary MM (2016) Mineralogical and petrographical study of the Duwi Formation Phosphorite. *Bull Natl Res Centre* 41(1):359–370
- Abou El-Anwar EA, Mekky HS, Abd El Rahim SH (2020) Discovery of spherulitic dahllite associated with carbonates at Hamadat phosphorite mine, Qusseir, Central Eastern Desert, Egypt. *Carbonates Evaporites* 35:106. <https://doi.org/10.1007/s13146-020-00637-x>
- Adegoke AK, Abdullah WH, Hakimi MH, Yandoka BMS, Mustapha KA, Aturamu AO (2014) Trace elements geochemistry of kerogen in Upper Cretaceous sediments, Chad (Bornu) Basin, northeastern Nigeria: origin and paleo-redox conditions. *J Afr Earth Sci* 100:675–683
- Akyuz T, Akyuz S, Calglar H, Calgar N (2008) FT-IR, EDXRF analysis of the mardin-mazidag phosphate deposit of turkey and relations between phosphate, uranium and fluorine. *Asian J Chem* 20(5):4085–4091
- Algeo T, Tribovillard N (2009) Environmental analysis of paleoceanographic systems based on molybdenum-uranium covariation. *Chem Geol* 268:211–225
- Altschuler ZS (1980) The geochemistry of trace elements in marine phosphorites. Part I. Characteristics, abundances and enrichment. *The Society of Economic Paleontologists and Mineralogists (SEPM) vol 29 SEPM Spec Publ*, Tulsa, 19–30
- Baioumy HM, Tada R (2005) Origin of upper cretaceous phosphorites in Egypt. *Cretac Res* 26:261–275
- Bata T (2016) Evidences of widespread cretaceous deep weathering and its consequences: a review. *Earth Sci Res* 5(2):69
- Batarseh M, El-Hasan T (2009) Toxic element levels in the phosphate deposits of central Jordan, *Soil and Sediment Contamination. An Int J* 18(2):205–215
- Bots P, Behrends T (2008) Uranium mobility in subsurface aqueous systems: the influence of redox conditions. *Miner Mag* 72:381–384
- Canadian Food Inspection Agency, Plant Production: fertilizers section, (1997) Website: www.inspection.gc.ca/English/plaveg/fereng/tememo/t-4-83.shtml
- Caspari T (2006) Geochemical investigation of soils developed in different lithologies in Bhutan, Eastern Himalayas. *Geoderma* 136:436–458
- Chen J, Algeo TJ, Zhao L, Chen Z-Q, Cao L, Zhang L, Li Y (2015) Diagenetic uptake of rare earth elements by bioapatite, with an example from Lower Triassic conodonts of South China. *Earth Sci Rev* 149:181–202
- de Silva EFD, Ammar M, Celso G, Fernando N, Abdelkrim C, Cristina S, Valdemar E, Ana R, Marques F (2010) Heavy elements in the phosphorite from Kalaat Khasba mine (North-western Tunisia): potential implications on the environment and human health. *J Hazard Mater* 182:232–245
- Deditius AP, Utsunomiya S, Reich M, Kesler SE, Ewing RC, Hough R, Walshe J (2011) Trace metal nanoparticles in pyrite. *Ore Geol Rev* 42:32–46
- Delian F, Tao Z, Jie Y, Yea J, Kribekc B, Dobesc P, Varrinc P, Zak K (2004) Geochemistry and origin of tin–polymetallic sulfide deposits hosted by the Devonian black shale series near Dachang, Guangxi, China. *Ore Geol Rev* 24:103–120
- El-Kammar AM, Zayed M, Amer SA (1979) Rare earths of the Nile Valley phosphorites, Upper Egypt. *Chem Geol* 24:69–81
- El-Tarabili E (1969) Paleogeography, paleoecology and genesis of the phosphatic sediments in the Quseir-Safaga region, UAR. *Econ Geol* 64:172–182
- Eskenazy GM (2009) Trace elements geochemistry of the Dobrudza coal basin, Bulgaria. *Int J Coal Geol* 78:192–200
- European Commission (EC) (1986) Council Directive (86/278/EEC) on the protection of the environment, and in particular of soil, when sewage sludge is used in agriculture. *Official J European Community, L* 181 (Annex 1A) 6–12
- Fedo CM, Eriksson K, Krogstad EJ (1996) Geochemistry of shale from the Archean (~ 3.0 Ga) Buhwa greenstone belt, Zimbabwe: implications for provenance and source area weathering. *Geochim Cosmochim Acta* 60(10):1751–1763
- Galarraga F, Reategui K, Martínez A, Martínez M, Llamas JF, Márquez G (2008) V/Ni ratio as a parameter in palaeo-environmental characterization of non-mature medium-crude oils from several Latin American basins. *J Petrol Sci Eng* 61:9–14
- Gallego-Torres D, Martinez-Ruiz F, De Lange GJ, Jimenez-Espejo FJ, Ortega-Huertas M (2010) Trace-elemental derived paleoceanographic and paleoclimatic conditions for Pleistocene Eastern Mediterranean sapropels. *Palaeogeogr Palaeoclimatol Palaeoecol* 293(1):76–89
- Gao P, Zheng YF, Zhao ZF (2016) Distinction between S-type and peraluminous I type granites: zircon versus whole-rock geochemistry. *Lithos* 258–259:77–91
- Glenn C, Arthur A (1990) Anatomy and origin of a Cretaceous phosphorite green sand giant. *Egyptian Sedimentol* 37:132–154
- Jiang YB, Ji HB (2012) Rare earth geochemistry in the dissolved, suspended and sedimentary loads in Karstic Rivers, Southwest China. *Environ Earth Sci* 66(8):2217
- Jones B, Manning DA (1994) Comparison of geochemical indices used for the interpretation of palaeoredox conditions in ancient mudstones. *Chem Geol* 111:111–129
- Khorasanipour M, Jafari Z (2018) Environmental geochemistry of rare earth elements in Cu-porphry mine tailings in the semiarid climate conditions of Sarcheshmeh mine in southeastern Iran. *Chem Geol* 477:58–72
- Kohn MJ, Moses RJ (2013) Trace element diffusivities in bone rule out simple diffusive uptake during fossilization but explain in vivo uptake and release. *Proc Natl Acad Sci* 110:419–424. <https://doi.org/10.1073/pnas.1209513110>
- Lécuyer C, Reynard B, Grandjean P (2004) Rare earth element evolution of Phanerozoic seawater recorded in biogenic apatites. *Chem Geol* 204:63–102
- McLennan SM (1993) Weathering and global denudation. *J Geol* 101(2):295–303
- Narula S, Wellington J (2007) Multiple criteria linear regression. *Eur J Operat Res* 181(2):767–772

- Nesbitt HW, Young GM (1982) Early Proterozoic climates and plate motions inferred from major element chemistry of lutites. *Nature* 199:715–717
- Ozer A, Gulaboglu K, Bayrakceken MS (2000) Physical structure and chemical and mineralogical composition of the Mazidagi (Turkey) phosphate rock. *Ind Eng Chem Res* 39:679–683
- Pattan JN, Pearce NJG (2009) Bottom water oxygenation history in southeastern Arabian Sea during the past 140 ka: results from redox-sensitive elements. *Palaeogeogr Palaeoclimatol Palaeoecol* 280:396–405
- Peters KE, Moldowan JM (1993) *The biomarker guide: interpreting molecular fossils in petroleum and ancient sediments*. Prentice-Hall Inc, Englewood Cliffs
- Pi DH, Jiang SY, Luo L, Yang JH, Hong-Fei Ling HF (2014) Depositional environments for stratiform witherite deposits in the lower Cambrian black shale sequence of the Yangtze platform, southern Qinling region, SW China: evidence from redox-sensitive trace element geochemistry. *Palaeogeogr Palaeoclimatol Palaeoecol* 398:125–131
- Rudnick RL, Gao S (2014) Composition of the continental crust. *Treatise Geochem* 3:1–64
- Said R (1962) *The geology of Egypt*. Elsevier Publishing Co, Amsterdam, p 377
- Said R (1990) *The geology of Egypt*. Netherlands, A.A, Balkema, Rotterdam, p 734
- Schieber J, Baird G (2001) On the origin and significance of pyrite spheres in Devonian black shale of North America. *J Sedimentary Res* 71(1):155–166
- Sengul HA, Ozer K, Gulaboglu MS (2006) Beneficiation of Mardin-Mazidagi (Turkey) calcareous phosphate rock using dilute acetic acid solutions. *Chem Eng J* 122:135–140
- Shi C, Cao J, Bao J, Zhu C, Jiang X, Wu M (2015) Source characterization of highly mature pyrobitumens using trace and rare earth element geochemistry: sinian-paleozoic paleo-oil reservoirs in south China. *Org Geochem* 83–84:77–93
- Spear DA, Zheng Y (1999) Geochemistry and origin of elements in some UK coals. *Int J Coal Geol* 38:161–179
- Song HJ, Wignall PB, Tong JN, Bond DPG, Song HY, Lai XL, Zhang K, Wang HM, Chen YL (2012) Geochemical evidence from bioapatite for multiple oceanic anoxic events during Permian-Triassic transition and the link with end-Permian extinction and recovery. *Earth Planet Sci Lett* 323–324:12–21
- Taylor SR, McLennan SM (1985) *The continental crust: its composition and evolution*. Blackwell, Oxford, p 312p
- Temraz MG (2005) *Mineralogical and geochemical studies of carbonaceous shale deposits from Egypt*. PhD Thesis, Berlin University, p 124
- Turekian KK, Wedepohl KH (1961) Distribution of the elements in some major units of the earth's crust. *Bull Geol Soc Am* 72:175–192
- Venter R, Boylett M (2009) The evaluation of various oxidants used in acid leaching of uranium. *Hydrometallurgy Conference, The Southern African Institute of Mining and Metallurgy* 445–456
- Waite TD, Davis JA, Payne TE, Waychunas GA (1994) Uranium (VI) adsorption to ferrihydrite: application of a surface complexation model. *Geochim Cosmochim Acta* 58:5465–5478
- Wignall PB, Twitchett RJ (1996) Oceanic anoxia and the end Permian mass extinction. *Science* 272:1155–1158
- Youssef MI (1957) Upper Cretaceous rocks in Quseir area. *Bull Inst Desert Egypt* 35–547
- Yusoff ZM, Ngwenya BT, Parsons I (2013) Mobility and fractionation of REEs during deep weathering of geochemically contrasting granites in a tropical setting, Malaysia. *Chem Geol* 349:71–86
- Zhang L, Algeo TJ, Cao L, Zhao L, Chen Z-Q, Li Z (2016) Diagenetic uptake of rare earth elements by conodont apatite. *Palaeogeogr Palaeoclimatol Palaeoecol* 458:176–197

Publisher's Note Springer Nature remains neutral with regard to jurisdictional claims in published maps and institutional affiliations.